Noname manuscript No.
(will be inserted by the editor)

Simulation Studies of DFB Laser Longitudinal Structures for Narrow Linewidth Emission

Heikki Virtanen · Topi Uusitalo · Mihail Dumitrescu

Received: date / Accepted: date

Abstract The paper presents simulation studies targeting high-power narrow-linewidth emission from semiconductor distributed feedback (DFB) lasers. The studies contain analytic and numerical calculations of emission linewidth, side mode suppression ratio and output power for DFB lasers without phase shifts and with $1\times\lambda/4$ and $2\times\lambda/8$ phase shifts, taking into account the grating and facets reflectivies, the randomness of the spontaneous emission and the longitudinal photon and carrier density distributions in the laser cavity.

Single device structural parameter optimization is generally associated with a trade-off between achieving a narrow linewidth and a high output power. Correlated optimization of multiple structural parameters enables the evaluation of achievable ranges of narrow linewidth and high power combinations.

Devices with long cavities and low grating coupling coefficients, κ (keeping κL values below the levels that promote re-broadening), with AR-coated facets and with a distributed phase-shift have the flattest longitudinal photon and carrier density distributions. This flatness enables stable single-longitudinal-mode operation with high side-mode-suppression ratio up to high injection current densities, which facilitates narrow linewidths and high output powers.

The results reported in the paper indicate that Master-Oscillator Power-Amplifier (MOPA) laser structures are needed for achieving W-level high-powers with sub-MHz linewidths because most single-cavity DFB laser structural variations that reduce the linewidth also limit the achievable output power in single-mode operation.

Keywords high power · narrow linewidth · distributed feedback laser

The research has been done within the European Space Agency project Sub-Megahertz Linewidth Laser for Fundamental Physics Missions (contract No. 4000110645/13/NL/HB).

H.Virtanen · T. Uusitalo · M. Dumitrescu
Optoelectronic Research Centre, Tampere University of Technology
P. O. Box 692, FIN-33101 Tampere, Finland
E-mail: heikki.a.virtanen@tut.fi

1 Introduction

Efficient high-power narrow-linewidth laser diodes are required for a broad range of applications, from sensing to LIDAR/DIAL and atomic clocks. The theory of semiconductor laser linewidth predicts that the intrinsic spectral width of a laser line is inversely proportional to the output power (Henry, 1982). On the other hand experimental observations have shown that there are several detrimental effects (nonlinear gain compression (Grillot et al, 2008), poor side mode suppression (Su et al, 2004; Coleman et al, 2012), spatial hole burning (Takaki et al, 2003)), that lead to linewidth re-broadening with increasing output power of distributed feedback (DFB) lasers.

To achieve high-power narrow linewidth emission without re-broadening effects, the DFB laser structural parameters require extensive optimization. The paper analyzes the effects of the grating length, coupling coefficient and phase-shifts on the carrier and photon densities along the DFB laser cavity and on the side-mode-suppression ratio (SMSR), output power and linewidth. The analysis takes into account the spontaneous emission noise, the gain compression and the effective refractive index variations with carrier density.

The paper is organized as follows. Section 2 provides the descriptions and theories behind the used analytic and numerical methods that have been exploited to analyze the effects of different parameters on the emission linewidth, SMSR, and the output power of DFB lasers without phase shifts and with $1\times\lambda/4$ and $2\times\lambda/8$ phase shifts. Section 3 is devoted to the analytic and numerical simulation results and comparisons. This section also includes discussions based on the results. Finally, Section 4 summarizes the most important results and draws the main conclusions.

2 Theory

According to the semiconductor laser theory, the intrinsic lineshape of a single-mode Fabry-Perot laser diode in steady state is Lorentzian with a linewidth given by (Henry, 1982; Coldren et al, 2012):

$$\Delta\nu = \frac{R_{sp}}{4\pi D}(1+\alpha_{H,eff}^2)K_c \tag{1}$$

$$= \frac{\hbar\omega_0\ v_g^2 n_{sp}(\alpha_i+\alpha_m)\alpha_m}{8\pi P_0}(1+\alpha_{H,eff}^2)K_c, \tag{2}$$

where R_{sp} is the average rate of spontaneous emission coupled into the lasing mode, D is the number of photons in the lasing mode, $\alpha_{H,eff}$ is the effective linewidth enhancement factor, K_c is the Petermann factor, v_g is the group velocity, n_{sp} is the population inversion factor, α_i is the internal loss factor per unit length, α_m is the distributed mirror loss factor per unit length, $\hbar$ is the reduced Planck constant, and ω_0 is the angular frequency. The output

power P_0 per facet and the threshold current I_{th} are given by:

$$P_0 = \frac{\hbar\omega_0\eta_i(I - I_{th})}{q}\frac{\alpha_m}{\alpha_i + \alpha_m} \quad \text{and } I_{th} = \frac{qV_{act}N_{th}}{\tau_c}, \tag{3}$$

where η_i is the internal quantum efficiency, I is the bias current, V_{act} is the active region volume, N_{th} is the threshold carrier density per unit volume, q is the elementary charge, and τ_c is the carrier lifetime that is calculated by:

$$\tau_c = \frac{1}{A + BN + CN^2}, \tag{4}$$

where A, B, and C are the monomolecular, bimolecular, and Auger recombination coefficients. N is the carrier density per unit volume.

The Petermann factor is defined as (Wang et al, 1987; Petermann, 2012):

$$K_c = \left| \frac{\int\int\int |\Psi(x,y,z)|^2 dV}{\int\int\int \Psi^2(x,y,z) dV} \right|^2, \tag{5}$$

where Ψ is the optical field amplitude in the laser cavity. The Petermann factor is induced by spontaneous emission noise from cavity eigenmodes homodyned into the lasing mode. Therefore, spontaneous emission sources with random Gaussian distribution in time and in the laser cavity were included in our time-domain traveling wave (TDTW) model.

Equation (2) indicates that a reduction in the internal losses leads to narrower emission linewidth. Hence, an optimized epilayer structure and doping profile, a low defect density, and low scattering losses (associated with high-quality low-order gratings) are crucial elements for obtaining a narrow linewidth emission. A reduction in the linewidth enhancement factor, $\alpha_{H,eff}$, through increasing the differential gain by red-shifting the gain peak with respect to the Bragg resonance wavelength, is also beneficial for emission linewidth narrowing. Equations (2) and (3) also indicate that the emission linewidth can be decreased by reducing the active region volume and increasing the internal quantum efficiency, which can be achieved by employing single quantum well active regions, by minimizing the lateral current leakage and the carrier escape from the active regions, and by reducing the non-radiative recombination rates. Also index-guided structures, that have Petermann factors close to unity, are more favorable than gain-guided lasers when narrow linewidth emission is targeted. Equations (2) and (3) point out that the emission linewidth can be substantially decreased by reducing the mirror losses, but that reduced mirror losses also diminish the output power. Thus, from the device structural design point of view related to mirror loss, a high output power and a narrow emission linewidth have a trade-off relation.

The mirror losses, which have a significant influence on the trade-off between achieving a high output power and achieving a narrow emission linewidth, have been evaluated by an analytic formula derived from the effective mirror theory (Coldren et al, 2012):

$$\alpha_m = \frac{\kappa}{4\tanh(\kappa L/2)} \ln\left(\frac{1}{R_{12}R_{34}}\right) \tag{6}$$

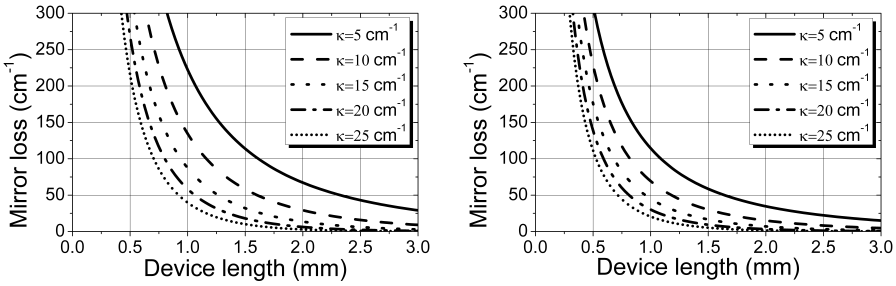

Fig. 1 DFB laser mirror loss variation with device length for different values of the coupling coefficient; evaluated according to Equation (6), using phase-matched end facet reflectivities R_1=R_2=1% for the left panel and $R_1 = 1\%$, $R_2 = 90\%$ for the right panel.

where $r_{12} = (r_1+r_2)/(1+r_1r_2)$, $r_{34} = (r_3+r_4)/(1+r_3r_4)$, $r_2 = r_3 = \tanh(\frac{\kappa L}{2})$, $R_{12} = r_{12}^2$, $R_{34} = r_{34}^2$, $r_1 = \sqrt{R_1}$, $r_4 = \sqrt{R_4}$, with κ the grating coupling coefficient, L the cavity length, and R_1 and R_4 the end facet reflectivities.

Fig. 1 shows the mirror loss variation with cavity length for different coupling coefficient values. The mirror losses were calculated with (6) for DFB lasers without phase shifts and for different phase-matched end facet reflectivities in the left and right panels. Fig. 1 illustrates that for short cavity lengths the mirror losses are dominated by the end facet reflections and by the coupling coefficient. For long device lengths the effects of the end facet reflections and of the coupling coefficient on the linewidth are significantly reduced and increasing the cavity length has more effect on linewidth narrowing.

2.1 Numerical modeling

The grating structure complicates the DFB laser simulation because the longitudinal photon and carrier density distributions can be highly non-uniform and differ significantly from the photon and carrier density distributions of a Fabry-Perot laser with the same end facet reflectivies. These non-uniformities introduce two main difficulties when Equation (2) and and (3) are applied to DFB lasers. First, due to the non-uniform photon density distribution, the relation between the total photon number and the facet output power is difficult to establish in an analytic form for an arbitrary cavity structure. The second difficulty comes from the evaluation of the mirror losses that also depend on the structure, which can include different phase-shifts, carrier-density-dependent effective refractive index distributions and can have longitudinal variations of the carrier and photon densities and of the coupling coefficient. The analytic mirror loss equation and the relation between the output power and the photon number can provide a good accuracy only when the κL-product is relatively low and the end facet reflections are dominant with respect to the optical feedback provided by the grating. Especially for high κL it is useful to compare

the results given by analytic equations to numerical simulations that can take into account the non-idealities and non-uniformities in the laser cavity.

The numerical simulations reported in the paper employed a time-domain traveling wave (TDTW) model, which takes into account the longitudinally non-uniform distributions of photon density, carrier density, gain, and effective refractive index; the spontaneous emission noise and the gain compression (Carroll et al, 1998; Piprek et al, 2005; Virtanen, 2015). The TDTW numerical method is based on solving the time-dependent traveling wave equations for counter-propagating slowly varying optical field envelopes F and R:

$$\frac{1}{v_g}\frac{\partial F(t,z)}{\partial t} + \frac{\partial F(t,z)}{\partial z} = (g - i\delta - \alpha_i)F(t,z) + i\kappa R(t,z) + s_F, \tag{7}$$

$$\frac{1}{v_g}\frac{\partial R(t,z)}{\partial t} - \frac{\partial R(t,z)}{\partial z} = (g - i\delta - \alpha_i)R(t,z) + i\kappa F(t,z) + s_R, \tag{8}$$

with the modal field gain g:

$$g(z,t) = \frac{\Gamma \frac{\partial g_m}{\partial N}(N(z,t) - N_{tr})}{2(1+\epsilon S)}, \tag{9}$$

where Γ is the optical confinement factor in the active region, ϵ is the gain compression factor, S is the photon density per unit volume, g_m is the material field gain per unit length, N_{tr} is the transparency carrier density per unit volume, and δ is the detuning factor that gives the deviation from the Bragg condition:

$$\delta = \frac{\omega_0}{c} n_{eff}(z,t) - \frac{\pi}{\Lambda}. \tag{10}$$

In Equation (10) c is the speed of light and Λ is the grating period of the DFB laser. n_{eff} is the effective refractive index (i.e. the refractive index experienced by the time-harmonic optical field when propagating along the structure) and its dependency on the carrier density is given by:

$$n_{eff}(z,t) = n_{eff,0} - \Gamma \alpha_{H,eff} \frac{\partial g_m}{\partial n}(N(z,t) - N_{tr}). \tag{11}$$

where $n_{eff,0}$ is the effective refractive index at the transparency carrier density. The spontaneous emission noise sources are Gaussians with zero mean and satisfy the following correlation relation:

$$\langle s_{F,R}(z,t), s^*_{F,R}(z',t')\rangle = \beta K_c (BN^2/L) v_g \hat{\delta}(z-z')\hat{\delta}(t-t') \tag{12}$$

where β is the spontaneous emission coupling factor and $\hat{\delta}$ is the delta function. Equations (7) and (8) are solved together with a carrier rate equation:

$$\frac{dN}{dt} = \frac{\eta_i I}{qV_{act}} - \frac{N}{\tau_c} - \frac{g_m(N - N_{tr})v_g S}{1+\epsilon S}, \tag{13}$$

in each time step and spatial mesh point along the longitudinal direction of the active region. The following boundary conditions:

$$F(t,0) = r_1 R(t,0) \quad \text{and } R(t,L) = r_4 F(t,L), \tag{14}$$

and zero initial conditions are applied. The photon density is normalized with:

$$S = |F| + |R|. \tag{15}$$

Although, the TDTW model can be used to evaluate the emission linewidth directly by taking a discrete Fourier transform from the time-domain output power, this is often cumbersome, particularly for narrow-linewidth lasers because it requires very long simulation times in order to average out the noise caused by spontaneous emission sources and reach a sufficient frequency resolution for the linewidth evaluation. Therefore, in the numerical studies reported in the paper, the intrinsic emission linewidth is evaluated using Equation (1) and (2) and time-averaged longitudinal carrier and photon densities that are calculated using the TDTW model. The spontaneous emission rate coupled into the lasing mode is estimated by:

$$R_{sp} = v_g g n_{sp}. \tag{16}$$

The total photon number in Equation (1) is calculated by integrating the numerically solved photon density over the length of the cavity. The internal loss factor, optical confinement factor, group velocity, and coupling coefficient are assumed to have a translational invariance along the device length in all calculations.

3 Results

The output power and the emission linewidth have been analytically evaluated for a DFB laser with no phase shifts and phase-matched 1%/90% end facet reflectivities as a function of the coupling coefficient and of the cavity length using Equations (2),(3), and (6). The other modeling parameters are given in Table 1.

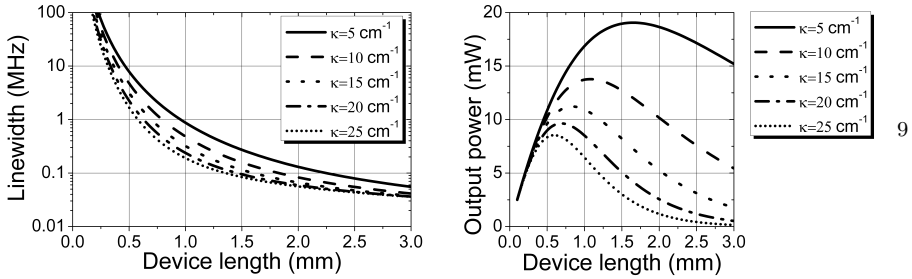

Fig. 2 Left panel: emission linewidth dependence on device length for different coupling coefficient values, calculated using Equations (2),(3), and (6). Right panel: output power dependence on device length for different coupling coefficient values, calculated using Equations (3) and (6). The end facet reflectivities are 1% and 90% and the injection current density is 6.25 kA/cm^2 in all cases.

The left panel of Fig. 2 indicates that the emission linewidth is more dependent on the coupling coefficient for short device cavity lengths, whereas the cavity length counts more for linewidth narrowing at long cavities. These relations derive from the dependencies of the mirror losses on the coupling coefficient and device length presented in Fig. 1. The right panel of Fig. 2 illustrates the dependency of the output power on the cavity length for different coupling coefficients. For a constant coupling coefficient at short cavity lengths the threshold current density decrease with cavity length influences more the output power than the extraction efficiency decrease with cavity length, whereas the reduced extraction efficiency and, correspondingly, the smaller slope efficiency are more important at long cavity lengths. Hence, there is an optimum cavity length where the output power has a maximum, beyond which the output power decreases with cavity length. The maximum power decreases with increased coupling coefficient since the advantage of threshold current density decrease is overcome by reduced extraction efficiency for shorter cavities and at lower output power as the extraction efficiency diminishes faster with cavity length when the coupling coefficient is higher.

Fig. 3 gives a comparison of the emission linewidth and output power variations with device length calculated using Equations (2),(3), and (6) and determined by TDTW simulations. The calculations have been performed at a current density of 6.25 kA/cm^2, for a small coupling coefficient, which mitigates re-broadening effects for long cavities.

The left panel of Fig. 3 shows that the analytic method gives relatively similar linewidth values compared to the numerical method, particularly for short cavity lengths in the single-mode regime. The differences between the predicted linewidth values for longer cavity lengths are associated with the non-uniform longitudinal carrier and photon density distributions, which are not taken into account in the analytic calculations. The right panel of Fig. 3 shows that the TDTW model predicts smaller output powers for short device lengths and a faster increase of the output power with device length. The

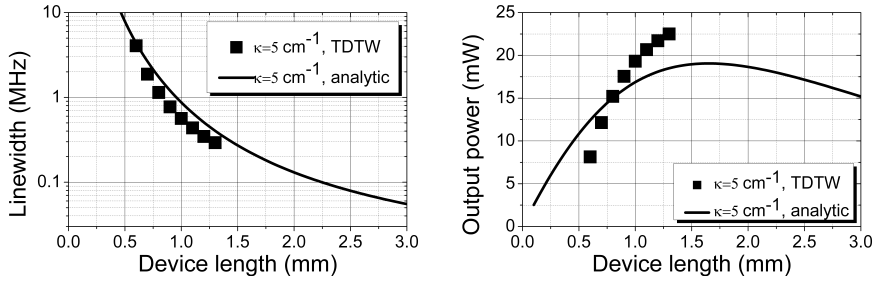

Fig. 3 Emission linewidth dependencies on device length (left panel) and output power dependencies on device length (right panel), calculated using the numerical TDTW model and the analytic Equations (2),(3), and (6) for an injection current density of 6.25 kA/cm^2. The results of the TDTW model were calculated only for device lengths that yielded side mode suppression ratios above 40 dB. The end facet reflectivities were 1% and 90% and the simulated devices did not have phase-shifts.

differences are derived from the round-trip gain and mirror loss calculations that are implicitly embedded into the TDTW model. The TDTW simulations illustrate that the single-mode regime is limited by grating strength (κL) for short cavities and by spatial hole burning (SHB) at large device lengths.

Table 1 Simulation parameters

symbol	parameter	value
λ_0	emission wavelength	780 nm
$n_{eff,0}$	effective refractive index	3.35
n_g	group index	4.0
W	ridge width	2 μm
d	thickness of the guiding area	0.2 μm
Γ	optical confinement factor	0.025
α_i	internal loss factor	12 cm^{-1}
A	monomolecular recombination coefficient	0 s^{-1}
B	bimolecular recombination coefficient	1×10^{-10} cm^3 s^{-1}
C	Auger recombination coefficient	3×10^{-29} cm^6 s^{-1}
N_{tr}	transparency carrier density	3.47×10^{18} cm^{-3}
$\frac{\partial g_m}{\partial N}$	differential gain	4.5×10^{-16} cm^2
$\alpha_{H,eff}$	effective linewidth enhancement factor	4.0
n_{sp}	population inversion factor	2
β	spontaneous emission coupling factor	2.8705×10^{-6}
η_i	internal quantum efficiency	0.5
ϵ	gain compression factor	1.0×10^{-17} cm^3
K_c	Petermann factor	1
J	injection current density	6.25 $\mathrm{kA/cm}^2$

The SHB effect can be observed in Fig. 4, which shows longitudinal carrier and photon density distributions. In the DFB laser with no phase shifts and 1%/90% end facet reflectivities the photon density at the AR-coated output facet (placed at 0 mm in the cavity) decreases as the coupling coupling coef-

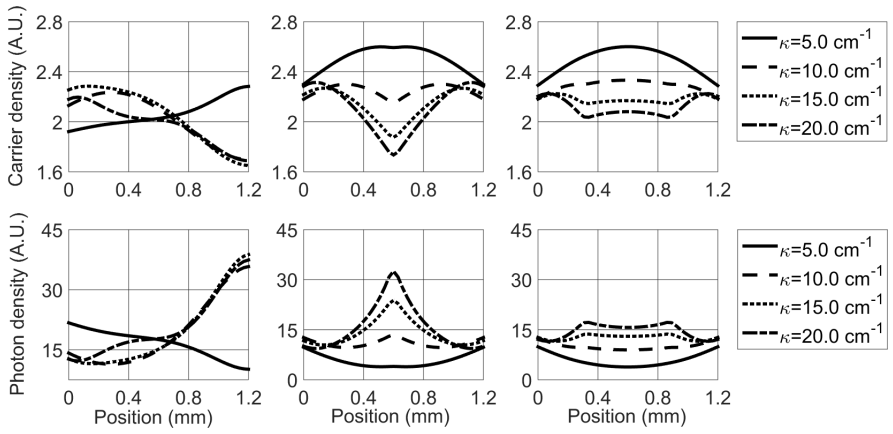

Fig. 4 Longitudinal relative carrier density (top panels) and photon density (bottom panels) distributions in a DFB laser with no phase shifts and phase-matched 1%/90% end facet reflectivities (left panels) and in DFB lasers with $1\times\lambda/4$ and with $2\times\lambda/8$ phase-shifts and phase-matched 1%/1% end facet reflectivities (middle and right panels, respectively). The distributions are simulated with the TDTW model at 6.25 kA/cm^2 injection current density. The other simulation parameters are given in Table 1.

ficient increases. When the increasing coupling coefficient results in a grating reflectivity close to the reflectivity of the HR-coated end facet (placed on the right side in the panels of Fig. 4), the photon lifetime in the region next to the HR-coated facet increases, leading to a switch in the asymmetrical longitudinal distributions of the carrier and photon densities, which induces a saturation and even a decrease in the single-mode output power. If the coupling coefficient is increased to a value that results in a higher grating reflectivity than the HR-coated end facet, the output power at the AR-coated end facet can also increase but this happens due to multi-mode operation that exploits the highly non-uniform longitudinal carrier density.

Fig. 4 indicates that DFB laser structures with $2\times\lambda/8$ phase-shifts, AR/AR coated end facets and grating strengths around 1 lead to the flattest carrier and photon density distributions. This enables single-mode operation up to higher current densities, which lead to narrower linewidths and higher output powers. Higher grating strengths increase the non-uniformity of the carrier and photon density distributions, which can deplete the gain of the strongest lasing mode, reduce the side-mode-suppression-ratio and ultimately lead to multi-mode operation at lower current densities.

Table 2 gives linewidth and output power values calculated with Equations (2),(3), and (6) and determined by TDTW simulations for pairs of κ and L values that correspond to a few values chosen for κL.

Table 2 Side-mode-suppression ratio, linewidth ($\Delta\nu^{\mathrm{a}}$ and $\Delta\nu^{\mathrm{n}}$) and output power ($\mathrm{P}_0^{\mathrm{a}}$ and $\mathrm{P}_0^{\mathrm{n}}$) values calculated using analytic equations and simulated using the TDTW model, respectively, for DFB lasers without phase shifts and with 1%/90% phase-matched facet reflectivities and for DFB lasers with $1\times\lambda/4$ and $2\times\lambda/8$ phase-shifts and with 1%/1% phase-matched facet reflectivities. The current density is kept constant at 6.25 kA/cm^2. The side-mode-suppression ratios are simulated with the TDTW numerical method. The coupling coefficients are in cm^{-1}, the device lengths are in cm, the calculated linewidths are in MHz, the output powers is are in mW and the SMSR values are in (dB).

PS	κL	κ	L	$\Delta\nu^{\mathrm{a}}$	$\Delta\nu^{\mathrm{n}}$	$\mathrm{P}_0^{\mathrm{a}}$	$\mathrm{P}_0^{\mathrm{n}}$	SMSR
0	1.3	5	0.260	0.0565	0.0504	19.469	26.637	1.4110
		10	0.130	0.1484	0.2668	16.993	15.474	3.6066
		15	0.087	0.2829	0.4887	15.076	10.075	52.581
		20	0.065	0.4671	0.8166	13.547	9.1276	52.053
	0.9	5	0.180	0.1090	0.1239	24.092	24.837	3.6926
		10	0.090	0.3462	0.5768	19.114	17.113	52.387
		15	0.060	0.7561	1.6853	15.841	11.011	50.313
		20	0.045	1.3830	5.2935	13.525	5.9929	38.215
	0.5	5	0.100	0.4093	0.5619	25.083	19.313	42.727
		10	0.050	1.8127	0.6225	16.857	5.7134	49.311
		15	0.033	4.7950	1018.4	12.694	0.0587	0.4149
		20	0.025	9.9411	1581.9	10.179	0.0395	0.1293
$\lambda/4$	1.3	5	0.260	0.0731	0.1706	16.778	22.879	3.9102
		10	0.130	0.2278	0.4990	13.439	13.910	52.224
		15	0.087	0.4912	1.5063	11.208	8.2633	53.315
		20	0.065	0.8903	4.4481	9.6131	4.2009	52.649
	0.9	5	0.180	0.1688	0.5158	18.973	18.424	6.6513
		10	0.090	0.6674	2.6350	13.496	6.7625	50.665
		15	0.060	1.6625	1037.6	10.472	0.0297	8.9381
		20	0.045	3.3211	1894.6	8.5562	0.0192	1.8447
	0.5	5	0.100	0.8728	4.1753	16.866	5.0232	36.212
		10	0.050	4.7486	1791.6	10.225	0.0206	0.2742
		15	0.033	13.835	2616.0	7.3372	0.0158	0.4894
		20	0.025	30.342	4069.8	5.7210	0.0142	1.4584
$2\times\lambda/8$	1.3	5	0.260	0.0731	0.1513	16.778	22.752	3.1441
		10	0.130	0.2278	0.5509	13.439	14.082	52.474
		15	0.087	0.4912	1.9545	11.208	7.5650	52.478
		20	0.065	0.8903	8.1576	9.6131	2.7423	50.584
	0.9	5	0.180	0.1688	0.3257	18.973	19.110	42.679
		10	0.090	0.6674	3.0409	13.496	6.1046	50.239
		15	0.060	1.6625	1143.5	10.472	0.0266	1.5386
		20	0.045	3.3211	2064.8	8.5562	0.0186	1.1834
	0.5	5	0.100	0.8728	4.3888	16.866	4.9777	42.158
		10	0.050	4.7486	1407.4	10.225	0.0202	0.3507
		15	0.033	13.835	3826.5	7.3372	0.0153	1.0418
		20	0.025	30.342	4540.3	5.7210	0.0139	0.0166

The values in Table 2 illustrate that at constant κL the longer devices with smaller κ yield narrower linewidths and higher output powers. Also, when comparing the devices with the same phase-shift structure, a higher value of κL, but below the level that induces re-broadening, induces narrower linewidths. The equal linewidth and output power values given by analytic calculations for laser structures that differ only in terms of having one or two phase-shifts point out that the analytic approach does not take into account the effects

of the non-uniform longitudinal carrier and photon density distributions. Also the analytic approach does not enable a reasonably accurate evaluation of the SMSR.

It should be noted that the sometimes better performances evaluated for the DFB laser structures with no phase-shifts are a result of the fact that both the analytic calculations and the TDTW simulations assume phase-matching of the facet reflectivities. Consequently, the 90% facet reflectivity phase-matched with the grating reflectivities contributes substantially to improved characteristics. However, in practice the position of the cleaved facets cannot be accurately controlled with respect to the gratings, which results in a randomly distributed phase difference between the grating and facet reflectivities. This random phase difference induces a random distribution in the laser characteristics and is one of the main reasons for employing a binning process for the fabricated lasers, which groups the devices in performance categories. It can be concluded that, based both on the industrial practice and on several studies (Laakso et al, 2011) that the DFB laser structures with no phase-shifts and AR/HR-coated facets should be avoided when a high fabrication yield of devices with precise and controllable characteristics is required.

Fig. 5 illustrates that, when moving from DFB laser structures with no phase-shifts and phase-matched AR/HR-coated facets to DFB laser structures with $1\times\lambda/4$ phase-shift and AR/AR-coated facets and then to DFB laser structures with $2\times\lambda/8$ phase-shifts and AR/AR-coated facets, the device length range of single-mode operation with high SMSR increases and moves to higher cavity lengths and higher values of κL, while the minimum achievable emission linewidth decreases. This is largely due to flatter longitudinal carrier and photon density distributions. The higher output power simulated for the structure with no phase-shifts is a result of the phase-matched HR facet.

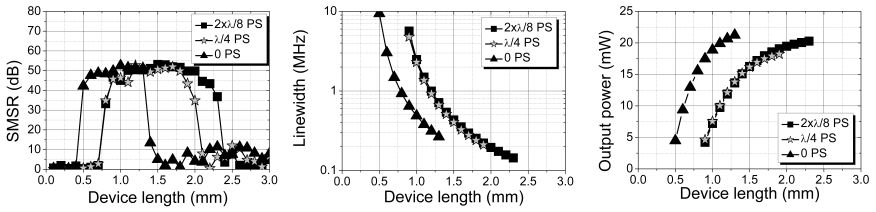

Fig. 5 Side mode suppression ratio (left panel), linewidth (middle panel) and output power (right panel) variations with device length for DFB lasers with no phase-shift and 1%/90% facet reflectivities and for DFB lasers with $1\times\lambda/4$ and $2\times\lambda/8$ phase shifts and 1%/1% facet reflectivities. The coupling coefficient is 7.5 cm^{-1} in the calculations.

Fig. 6 shows linewidths and output power variations with increasing device length for two values of κ, simulated with the TDTW model for DFB laser structures with no phase-shifts and phase-matched 1%/90%-coated facets, with $1\times\lambda/4$ phase-shift and 1%/1%-coated facets and with $2\times\lambda/8$ phase-shifts and 1%/1%-coated facets. The calculations have been performed for the same

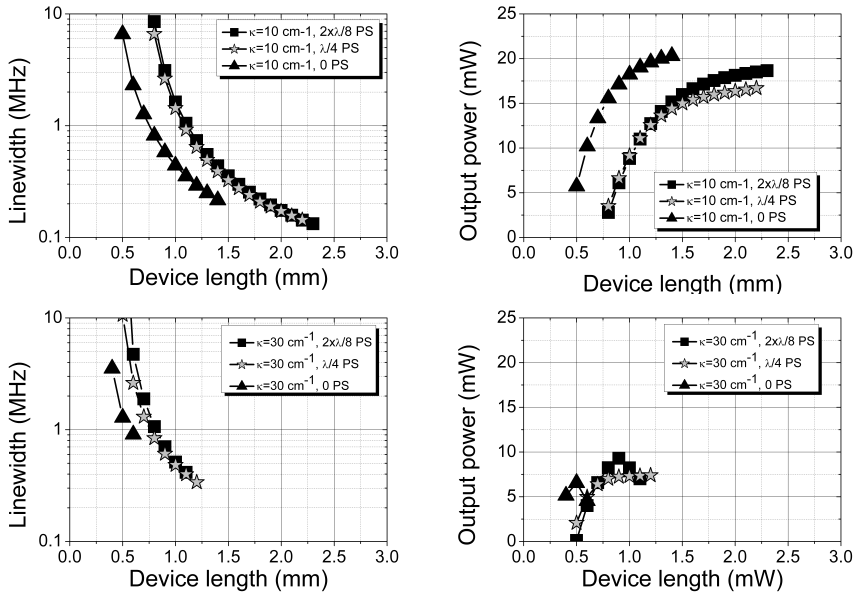

Fig. 6 Emission linewidths (left panels) and output powers (right panels) calculated with the TDTW numerical method for DFB lasers with no phase-shifts (PS) and 1%/90% phase-matched facet reflectivities and for DFB lasers with $1\times\lambda/4$ and $2\times\lambda/8$ phase-shifts and 1%/1% facet reflectivities. The simulations have been performed for κ=10 cm^{-1} (top panels) and for κ=30 cm^{-1} (bottom panels). The points are plotted only for single-longitudinal mode operation with side-mode-suppression ratios above 35 dB.

6.25 kA/cm^2 current density and the results have been plotted only for the ranges where the SMSR exceeded 35 dB. The plots of Fig. 6 support the conclusions that the use of phase-shifts extends the range of stable single-mode operation with high SMSR to longer cavities, which decreases the narrowest achievable linewidth. It is also apparent that smaller κ values enable achieving narrower linewidths and higher powers, also due to maintaining single-mode operation for longer device lengths. These conclusions are consistent with the fact that both the phase-shifts and the smaller values of κ induce flatter longitudinal distributions of carrier and photon densities (as illustrated in Fig. 4). The fact that the DFB laser structures with no phase-shifts might sometimes have better evaluated performances (like enabling higher output power, as shown in the right panel of Fig. 5 and in the top-right panel of Fig. 6) is derived from the assumption that the HR end facets are phase-matched with the gratings (which is only randomly occurring in real devices).

The output power decrease with increasing device length for the DFB laser structures with no phase-shifts and AR/HR phase-matched facet reflectivities, illustrated in the bottom-right panel of Fig. 6, corresponds to the switching of the asymmetrical photon and carrier longitudinal distributions, illustrated in the left panels of Fig. 4, which occurs when the grating reflectivity becomes comparable with the HR facet reflectivity.

4 Conclusions

The simulation studies presented in the paper show that the analytic evaluation of linewidth and output power leads to significant inaccuracies when the effects of the non-uniform longitudinal distributions of photon and carrier densities, gain, coupling coefficient and/or effective refractive index are important (which happens particularly for long cavities, large coupling coefficient values and/or under high injection levels). The implemented numerical TDTW model enabled more accurate evaluations, by taking into account the effects of longitudinal non-uniformities, spontaneous emission noise and gain compression.

The simulation results point out that the optimization through single parameter variation (e.g. by changing the cavity length or by changing the grating coupling coefficient) usually implies a trade-off between achieving a narrow linewidth and achieving a high output power. Correlated optimization of multiple parameters, for example increasing the cavity length while keeping a constant grating strength (κL=const.), might enable simultaneous linewidth narrowing and output power increase in single-mode operation.

Increasing κ for constant cavity lengths continuously narrows the linewidth, while increasing the output power up to a maximum, followed by a decrease in the output power. Increasing L while keeping κ constant also continuously narrows the linewidth, while inducing an increase in the output power for short devices, up to a maximum, followed by an output power decrease for long cavity devices. The maximum achievable output power, for a given current density and variable cavity length, decreases for higher κ values and occurs at shorter cavities. Longer cavities and smaller κ lead to narrower linewidths and higher output powers for constant κL at given current densities.

The presented simulation studies have also shown that long cavities with relatively low coupling coefficients, which keep the grating strength below the level which promotes re-broadening, combined with distributed phase-shifts and AR/AR-coated facets, have the flattest longitudinal photon and carrier density distributions. This flatness supports single longitudinal mode operation up to higher current densities, which enables achieving narrower linewidths and higher output powers.

Even with optimized structures some certain combinations of linewidth and output power levels cannot be achieved. The achievable ranges of linewidth and output power values identified by our simulation and experimental studies for 780 nm DFB lasers, intended for Rubidium atomic clocks, indicate that Master-Oscillator Power-Amplifier (MOPA) laser structures are needed for achieving W-level output powers with sub-MHz linewidths. In MOPA structures the master oscillator DFB section delivers a narrow linewidth single mode injection at tens of mW power level and the power amplifier section boosts the output power to W level. An important advantage of the MOPA structure is that the emission wavelength tuning and the output power level can be controlled independently through the master oscillator and power amplifier currents, respectively.

A more accurate analysis would require improved dispersion models for the material gain and for the effective refractive index, the evaluation of the longitudinal temperature distribution, and a modified linewidth equation that takes into account the contributions of various linewidth re-broadening effects to the emission linewidth.

References

Carroll JE, Whiteaway J, Plumb D (1998) Distributed feedback semiconductor lasers, vol 10. IET, London

Coldren LA, Corzine SW, Mashanovitch ML (2012) Diode lasers and photonic integrated circuits, vol 218. Wiley

Coleman JJ, Bryce AC, Jagadish C (2012) Advances in semiconductor lasers, vol 86. Academic Press

Grillot F, Dagens B, Provost JG, Su H, Lester LF (2008) Gain compression and above-threshold linewidth enhancement factor in 1.3-$\mu\{m\}$ InAs–GaAs Quantum-Dot Lasers. IEEE Journal of Quantum Electronics 44(10):946–951

Henry CH (1982) Theory of the linewidth of semiconductor lasers. IEEE Journal of Quantum Electronics 18(2):259–264

Laakso A, Karinen J, Telkkälä J, Dumitrescu M (2011) The effect of facet reflections in index-coupled distributed feedback lasers with coated facets. Optical and Quantum electronics 42(11-13):713–719

Petermann K (2012) Laser diode modulation and noise, vol 3. Springer, Berlin

Piprek J, et al (2005) Optoelectronic devices. Springer, Berlin

Su H, Zhang L, Wang R, Newell T, Gray A, Lester L (2004) Linewidth study of inas-ingaas quantum dot distributed feedback lasers. IEEE Photonics Technology Letters 16(10):2206–2208

Takaki K, Kise T, Maruyama K, Yamanaka N, Funabashi M, Kasukawa A (2003) Reduced linewidth re-broadening by suppressing longitudinal spatial hole burning in high-power 1.55-μm continuous-wave distributed-feedback (CW-DFB) laser diodes. IEEE Journal of Quantum Electronics 39(9):1060–1065

Virtanen H (2015) Time-domain travelling wave modelling of dual-wavelength DFB lasers in remote heterodyne detection links. Master's thesis, Tampere University of Technology, Tampere, Finland, Retrieved from http://URN.fi/URN:NBN:fi:tty-201505271422

Wang J, Schunk N, Petermann K (1987) Linewidth enhancement for dfb lasers due to longitudinal field dependence in the laser cavity. Electronics Letters 23(14):715–717